

# Methods to Characterise Exoplanet Host Stars from Spectroscopy

Carina M. Persson

**Abstract** A key to understand exoplanets is characterisation of their host stars. One of the most powerful tools to characterise stellar properties like effective temperature, surface gravity and metallicity, is spectroscopy based on observations of stellar atmospheres. This chapter describes the stellar parameters that can be derived from a spectrum with examples of well established methods and theoretical model atmospheres. Combined with photometry and parallax measurements, the outcome of the spectroscopic modelling can be used to derive stellar radii and masses.

## Introduction

Exoplanets are intimately connected to their host stars through formation and evolution. In addition, detection and characterisation of exoplanets depend on detailed knowledge of their host stars since the current major detection techniques, transit photometry and the radial velocity (RV) method, detect planet sizes and masses relative to their host star (see Chapters by Deeg & Alonso and Wright in Volume 1 of the Handbook of Exoplanets). Uncertainties in a host star's parameters propagate directly to the planets.

Stellar modelling is normally based on two major techniques – photometry and spectroscopy. These methods are model-dependent in contrast to the direct measurements by interferometry, eclipsing binaries, and asteroseismology.

For eclipsing binaries (e.g. Andersen 1991; Torres et al. 2010; Serenelli et al. 2021), and for the few large and nearby stars that enable interferometric measurements (e.g. Quirrenbach 2001; Eisenhauer et al. 2023), it is possible to derive the stellar radius with an accuracy of a few per cent. The timing of the duration of the eclipses of eclipsing binaries and their orbital velocities allows accurate estimates

---

Carina M. Persson

Chalmers University of Technology, department of Space, Earth, and Environment, Onsala space observatory, 439 92 ONSALA, Sweden, e-mail: [carina.persson@chalmers.se](mailto:carina.persson@chalmers.se)

of their sizes. Similarly, stellar masses can be accurately determined for visual binaries from observed separations from the common centre-of-mass with Kepler's third law that relates their masses with observed orbital period and separation. Asteroseismology can also be used to derive stellar mass, radius, and age with a high precision (see Chapter by Lundkvist, Huber, Aguirre & Chaplin in this volume of the Handbook of Exoplanets). Recently, the seismic surface gravity of the star has also been used to obtain the effective temperature and metallicity, in particular with APOGEE (Ahumada et al. 2020, 2022).

These methods are, however, currently only possible to apply to a small subset of all stars. Spectroscopic measurements open a window to derive stellar parameters from a larger pool of stars than from direct methods. High-resolution spectroscopy is a powerful tool that provides a wealth of information; the effective temperature, surface gravity, chemical composition, and velocities. The stellar radius, and the luminosity, can then readily be derived from its spectral energy distribution (SED) via the spectroscopic parameters combined with photometry and parallax.

The spectroscopic parameters also serve as a base to model characteristics that normally cannot be directly measured, like mass and age, with stellar evolution models and the complementary tool isochrones (e.g. Dotter 2016; Hidalgo et al. 2018). An isochrone is an evolutionary track for a population of stars with different masses on the Hertzsprung-Russell diagram with the same (*iso*) age (*chrone*). The mass and radius can also be obtained from the spectroscopic parameters and empirical calibration equations (e.g. Torres et al. 2010; Enoch et al. 2010; Southworth 2011) albeit often with a higher uncertainty.

The downside of high-resolution spectroscopy is that it is expensive; the observations are time-consuming and also requires bright stars or a large collecting area. Modelling of stellar parameters has therefore traditionally been performed by photometry because a much larger number of stars can quickly be observed and analysed. The effective temperature of a star can for instance be derived from color-color diagrams which have been scaled to stars measured with direct methods (e.g. Bell and Gustafsson 1989; Alonso et al. 1996; Nordström et al. 2004). However, such models have in general higher uncertainties than based on spectroscopic measurements. In that respect they may only be reliable in a statistical sense and not for individual stars. Thus for exoplanet host stars (for which direct measurements are not applicable), high-resolution spectroscopy is preferred.

This chapter begins with a short summary of a few basic requirements in order to obtain spectroscopic measurements of a star. It continues with an overview of the parameters that can be extracted from a high-resolution spectrum and a few examples of well established methods. Some advantages and caveats are highlighted. The chapter ends with a brief summary of how to combine spectroscopic parameters, photometric measurements, and stellar evolution models to obtain stellar radii and masses. Modelling of stellar ages are described by Christensen-Dalsgaard & Aguirre in a Chapter in this volume of the Handbook of Exoplanets.

## Instruments and spectral resolution

Important properties of a spectrum is high-resolution, high signal-to-noise (S/N), and wavelength coverage. There are several different types of spectrometers and many textbooks have been written about this topic including advantages and challenges for different types of instruments (e.g. Gray 2008). The most successful type in observations of exoplanets is echelle spectrographs. The main advantage is the high resolution combined with a wide wavelength coverage obtained in a single exposure. A description of high-precision cross-dispersed echelle spectrographs for exoplanet research (CORAVEL, ELODIE, CORALIE, SOPHIE and HARPS) is found in a Chapter by Francesco Pepe in this volume of the Handbook of Exoplanets.

For the purpose of spectroscopic modelling of host stars, we want high-resolution in order to resolve the spectral lines. The spectral resolution  $\Delta\lambda$  at wavelength  $\lambda$  is

$$\frac{\Delta\lambda}{\lambda} = \frac{1}{R}, \quad (1)$$

where  $R$  is the resolving power of the spectrograph. It can be translated into a velocity resolution according to

$$\Delta V = \frac{\Delta\lambda}{\lambda} c = \frac{c}{R}. \quad (2)$$

Doppler broadening of spectral lines due to thermal and turbulent motions of absorbing species in the atmospheres produce line widths of  $\sim 6 \text{ km s}^{-1}$  for late-type stars. This corresponds to a spectral resolution of 50 000. Low-mass, slowly rotating stars can have line widths of only  $\approx 1 - 2 \text{ km s}^{-1}$  which require  $R \gtrsim 300\,000$  to resolve the spectral lines and disentangle blended lines.

In terms of high resolution, ultra-high precision, and long-term stability, the High Accuracy Radial Velocity Planet Searcher (HARPS; Mayor et al. 2003) and its decade younger sibling HARPS-North (Cosentino et al. 2012) mounted on the ESO 3.6 m telescope (La Silla observatory, Chile) and the Telescopio Nazionale Galileo (TNG) of Roque de los Muchachos Observatory (La Palma, Spain), respectively, have been the leading instruments in detecting exoplanets over the last two decades. Both HARPS instruments are fiber-fed cross-dispersed high-precision echelle spectrographs covering 380 nm to 690 nm. The spectroscopic resolution is approximately 115 000 at visual wavelengths corresponding to a velocity resolution of  $2.6 \text{ km s}^{-1}$ . The design is based on experience with the groundbreaking ELODIE and CORALIE instruments where the former was used to detect the first exoplanet 51 Peg b (Mayor and Queloz 1995). Both HARPS spectrographs can be considered as the “gold standard” when searching for exoplanets in RV data and are also used for characterisation of exoplanet host stars. When searching for exoplanets with the RV method, many measurements are collected, sometimes over a period over many years. The individual spectra can be co-added (after correcting for the peri-

odic changes in radial velocity) in order to increase the S/N enabling spectroscopic characterisation of the host star.

In addition to the HARPS spectrographs, there are many other instruments used for exoplanet detection that can also be used to characterise host stars e.g. ESPRESSO (Pepe et al. 2021), FIES (Telting et al. 2014), HIRES (Vogt et al. 1994), CHIRON (Tokovinin et al. 2013), TULL (Tull et al. 1995) with different resolutions operating at different wavelengths.

## Stellar properties from spectroscopy

Only a few parameters characterise a stellar atmosphere: the effective temperature ( $T_{\text{eff}}$ ), the surface gravity ( $\log g_*$ ), the overall metal abundance ( $[M/H]$ ), and atmospheric and rotational velocities.

The surface of a star is defined as the location where photons escape from the star which occurs at a characteristic optical depth of  $2/3$ . This occurs within the photosphere, the innermost  $\approx 500$  km of a star's atmosphere which overlies the opaque interior. The photospheric temperature and density varies with depth and depends on the surface gravity as well as the abundances and opacity of the gases. The Sun's photosphere has a temperature that varies between 4 400 K and 6 600 K with an effective temperature of 5 772 K, while the density is approximately  $3 \times 10^{-4} \text{ kg m}^{-3}$ , increasing with depth into the Sun. Other stars may have hotter or cooler photospheres. Spectral absorption lines originate from different depths and opacities within the photosphere. Weak and optically thin spectral lines, and the line wings of optically thick lines, originate essentially in the same layer as the continuum. In contrast, the cores of optically thick saturated lines develop in higher layers. An example is the core of the hydrogen  $\alpha$  line at 6562.81 Å which originates in the hotter and less dense chromosphere which lies on top of the photosphere, where the assumption of local thermal equilibrium (LTE) is no longer valid.

## Effective temperature

Stars are classified according to effective temperature from the hot O-stars, also called early-type stars, to the cool M-stars (late-type stars). If a star is on the main sequence, the effective temperature immediately signals which type of star it is along with typical mass and radius.

Instead of choosing a particular depth to define a star's surface temperature, the effective temperature is defined in terms of flux. The effective temperature is defined via the Stefan-Boltzmann law in terms of the total power per unit area, radiated by the star (e.g. Gray 2008)

$$\int_0^\infty \mathcal{F}_\nu d\nu = \sigma T_{\text{eff}}^4. \quad (3)$$

Here  $\mathcal{F}_v$  is the total flux passing through the star's surface and  $\sigma$  is the Boltzmann constant. The effective temperature is thus the temperature of a black body having the same power output per unit area as a star. It is related to the flux we measure at Earth,  $f_v$ , via (Gray 2008)

$$\int_0^\infty f_v dv = \left(\frac{R_\star}{d}\right)^2 \int_0^\infty \mathcal{F}_v dv = \left(\frac{\theta_\star}{2}\right)^2 \sigma T_{\text{eff}}^4, \quad (4)$$

where the left integral is the total radiative flux from the star received at the top of the Earth's atmosphere (bolometric flux),  $R_\star$  is the stellar radius,  $d$  is the distance, and  $\theta_\star$  is the angular diameter of the star. The effective temperature can hence be derived by measuring the angular size of the star from interferometry and the received flux at Earth over a wide spectral range. By combining the angular size with distance from parallax measurements, the linear radius of the star can be inferred for a wide range of spectral types nearly model-independent except for the dependence on the adopted limb-darkening coefficients and bolometric correction. Alternatively, if the radius of the star is known from e.g. eclipsing binaries and the distance from parallax measurements, this will give the angular size which then can be used to compute  $T_{\text{eff}}$ . Since the target stars have to be nearby to measure their angular sizes, interstellar absorption can be neglected. The infrared flux method (IRFM Blackwell and Shallis 1977; Blackwell et al. 1980; Bell and Gustafsson 1989; Blackwell et al. 1990; Casagrande et al. 2006, 2010) is based on observations of the angular size of the star and the measured infrared flux at the top of the Earth's atmosphere. The bolometric flux is derived taking into account the bolometric correction which gives the effective temperature.

In addition to the above methods,  $T_{\text{eff}}$  can also be derived from spectroscopy as described in the following section. However, it is worth highlighting that the temperature derived from spectroscopy is a microscopic value which is close to, but not exactly the same as the effective temperature due to its definition being a macroscopic description.

### Surface gravity

The surface gravity is an indication of the luminosity class of a star where V is the main sequence and I – IV is different types of giants. Thus surface gravity contains information of the size and age of a star. A low surface gravity immediately indicates that the star has left the main sequence.

The surface gravity of a star is defined by (e.g. Gray 2008)

$$g_\star = g_\odot \frac{M_\star}{R_\star^2}, \quad (5)$$

where  $g_\odot$  is the surface gravity of the Sun ( $2.740 \times 10^4 \text{ cm s}^{-2}$ ) and the radius,  $R_\star$ , and mass,  $M_\star$ , of the star are in solar units. The surface gravity is commonly measured in a logarithmic scale,  $\log g_\star$ , where the solar value is 4.44.

The surface gravity determines the gas density in the photosphere and is the spectroscopic parameter that has the highest impact on the stellar radius. Unfortunately,  $\log g_*$  is often poorly constrained by spectral analysis. Since the uncertainties of  $T_{\text{eff}}$  and metallicity can be strongly correlated with surface gravity this can lead to a significant source of systematic error in some analysis techniques.

## Metallicity

A star's chemical composition is an outcome of the nucleosynthesis by previous generations of stars. This is important when reconstructing star and planet formation history in our Galaxy. There is a large variation of metallicity, i.e. the abundance of all elements heavier than helium denoted with  $[M/H]$ , in the Milky Way up to about twice the solar value to hundreds of thousands of times lower than the solar value (e.g. Christlieb et al. 2004; Li et al. 2022; Nepal et al. 2024).

The chemical composition of a star is commonly fixed to the overall metallicity of a star relative to the Sun. The Grevesse et al. (2007), Asplund et al. (2009) and Lodders (2003) abundance scales for the Sun are currently the most adopted. However, individual abundances of a star may not follow solar composition and may require modelling of individual elemental abundances. Abundances are generally measured on a logarithmic scale normalised to the Sun where zero equals the Sun's metallicity. In the case of iron we have  $[\text{Fe}/H]_* = \log(\text{Fe}/H)_* - \log(\text{Fe}/H)_\odot$ . For example, an iron abundance of  $[\text{Fe}/H] = -0.5$  means that the abundance is  $10^{-0.5}$  relative to the Sun. Since iron is by far the most abundant species in a stellar atmosphere after hydrogen and helium, measurements of iron has become a proxy for the metallicity.

Stellar abundances is also important when modelling exoplanet interiors in particular rocky super-Earths without significant gaseous envelopes. The degeneracy of interior composition inferred from radius and mass measurements can for this type of planet be reduced assuming an interior structure with a differentiated iron core and a rocky mantle. In these cases, the host star abundances is often used as a proxy of the primary planet-building elements Fe, Mg, and Si, which are expected to be reflected in the planet composition, planet interior, and core mass fraction (Dorn et al. 2015; Acuña et al. 2023).

## Velocities

Thermal widths of spectral lines are only a fraction of the observed line widths for dwarf stars hotter than spectral type K0. The line widths are instead mainly governed by Doppler shifts produced by motions of the star's photospheric gases. The radial velocity of the star is only shifting the wavelengths of all spectral lines in the observed spectrum compared to the observations and can easily be corrected for. The velocity that dominates the line shape and width for hot stars is the projected equatorial rotational velocity of the star,  $V \sin i_*$ , where  $i_*$  is the inclination of the stellar rotation axis relative to the line of sight. It can be measured via the full width

at half maximum (FWHM) of a large number of optically thin and unblended lines not sensitive to pressure broadening. The line shapes are, however, also affected by turbulence from convective motion, granulation, high-order pulsations, stellar activity, and other types of local flows in the photosphere. Turbulence is represented in the models by the macro-turbulent velocity ( $V_{\text{mac}}$ ) that describes motions on scales larger than the mean free path within the photosphere that induce a change in the line shape; and the micro-turbulent velocity ( $V_{\text{mic}}$ ) that describes motions on scales smaller than the mean free path leading to increased line opacity (Gray 2008; Bruntt et al. 2010; Doyle et al. 2014). The latter velocity is a “fudge” factor originally introduced to reconcile observed and predicted equivalent widths (Mihalas 1978). It includes all remaining types of broadening mechanisms and is at present standard to include in analyses of solar-type stars. Both turbulent velocities depend on temperature and to a lesser extent on surface gravity. The micro-turbulent velocity has a width of the order of  $1 \text{ km s}^{-1}$  for dwarfs and several  $\text{km s}^{-1}$  for giants. For low-mass stars,  $V_{\text{mac}}$  and  $V \sin i_*$  have comparable widths of the order of a few  $\text{km s}^{-1}$ . As a reference, the Sun’s  $V \sin i_*$  is  $2 \text{ km s}^{-1}$  at the equator while hotter stars have much higher rotational velocities (tens to hundreds of  $\text{km s}^{-1}$ ).

## Methods for spectroscopic modelling

There are several ways to model a spectrum which can be divided into two main groups. The first is based on spectral synthesis. Here observations are fitted to a synthetic spectrum of stellar atmosphere models by comparison of line profiles. The second is a line-by-line analysis based on measured strengths of observed spectral lines, their equivalent widths (EWs). Detailed description of the physics can be found in many textbooks e.g. Gray (2008). Spectroscopic observations can also be compared to a library of spectra of well-characterised stars via for example interferometric measurements or spectroscopic binaries.

One major problem in spectroscopic analysis is to accurately determine the continuum which can introduce large errors. This is particularly difficult for poor spectra with low spectral resolution or low S/N. It also depends on the spectral type of the star and the wavelength region. The number of spectral lines increases towards shorter wavelengths for all types of stars. In addition, late-type stars have a much higher density of spectral lines than early-type stars arising from both atoms and molecules leading to blending and confusion of the continuum location. The higher temperatures of early-type stars ionize a large fraction of their atoms, leading to significantly fewer spectral features than low-mass stars. Differences in rotational velocities also affect the spectral line density. In contrast to late-type stars, the early types have very high rotational velocities which leads to very broad spectral lines that smear out spectral features. Thus solar-type stars (FGK) are the easiest stars to model, while high- and low-mass stars often entails a significantly higher degree of difficulty in the modelling. M-dwarfs have in addition generally a much longer period of high stellar activity than FGK stars, exacerbating the problems (e.g. Mignion

et al. 2023). This is unfortunate since M-dwarfs are popular exoplanet host stars due to their small masses and sizes which increase the exoplanet signals.

Care must be taken when selecting which spectral lines to model. A large set of narrow, non-blended spectral lines are preferred (unless modelling pressure broadened line wings, see below). If a spectral line becomes optically thick, the abundance of a species stops growing linearly with absorption depth. The characteristics of an optically thick line is a saturated line centre which flattens the bottom and broaden the line wings. Not all optically thin spectral lines may, however, be useful since a large number comes with poorly determined atomic parameters which are needed to compute synthetic spectra. This can be circumvented for solar-type stars if adopting new atomic parameters after comparing the lines from observations of the Sun.

### *Fitting observations to synthetic spectra*

Computations of a synthetic spectrum requires a model atmosphere based on solutions to the stellar structure equations to synthesize a spectrum. Most stellar atmosphere models are pre-calculated and tabulated on grids describing the profiles of the temperature, surface gravity and abundances as functions of atmospheric depth. Each layer in the model atmosphere is contributing to the formation of absorption line profiles in the final spectrum. Some widely used atmospheric model atmospheres are Atlas12 (Kurucz 2013), Atlas9 (Kurucz 1993a; Heiter et al. 2002), MARCS (Gustafsson et al. 2008) for cool and giant stars, and LL models (Shulyak et al. 2004) for hot main sequence stars. Line lists of atomic and molecular data needed in the computation can be provided by the Vienna Atomic Line Database (VALD3; Piskunov et al. 1995; Ryabchikova et al. 2015).

A radiative transfer code then computes a synthetic model spectrum of the star for the chosen set of stellar parameters ( $T_{\text{eff}}$ ,  $\log g_*$ ,  $[\text{Fe}/\text{H}]$ ,  $V \sin i_*$ ,  $V_{\text{mic}}$ ,  $V_{\text{mac}}$ ) which are matched against the observed spectra based on the spectral line shapes and strengths. The parameters generally affect either the line strength ( $T_{\text{eff}}$ ,  $\log g_*$ , abundances, and  $V_{\text{mic}}$ ) or the line shape ( $V_{\text{mac}}$ ,  $V \sin i_*$ , and the instrumental resolution). Degeneracies are stronger within the subsets.

The dependence of the line profile on the  $V_{\text{mac}}$  parameter is broadened line wings and a cusp-shaped core. Unfortunately, disentangling the effect on the line profile from  $V \sin i_*$  and  $V_{\text{mac}}$  is difficult, leading to a degeneracy between the two. Prior information of  $V \sin i_*$  may be obtained from time-resolved photometry, available for the known transiting planets, or from asteroseismology (cf. Doyle et al. 2014). If no prior information is available, calibration equations of both turbulent velocities are often used (e.g. Bruntt et al. 2010; Doyle et al. 2014) which allows modelling of  $V \sin i_*$ . Note that in order to properly model the different velocities above, it is imperative to take into account how the spectrograph itself broadens the lines. Spectral lines can also be pressure broadened through various mechanisms which further broaden the lines, e.g. the Balmer lines. Details of the various broadening mechanisms can be found in many textbooks such as Gray (2008).



There are many softwares that compute synthetic spectra to be used as a model constraint to interpret the observed spectrum. The popular open-source spectroscopic tool *iSpec* (Blanco-Cuaresma et al. 2014; Blanco-Cuaresma 2019) support several of the most well-known radiative transfer codes such as *Spectroscopy Made Easy* (SME; Valenti and Piskunov 1996; Piskunov and Valenti 2017; Wehrhahn et al. 2023), *SPECTRUM* (Gray and Corbally 1994), *Turbospectrum* (Plez 2012; de Laverny et al. 2012; Gerber et al. 2023), *Synthe/WIDTH9* (Kurucz 1993b), and *MOOG* (Snedden 1973) where the latter is based on the equivalent width method. The codes often adopt LTE and a plane-parallel geometry as default motivated by the fact that for main-sequence stars, the photosphere constitutes  $\ll 1\%$  of the stellar radius. A spherically symmetric geometry is on the other hand required for giant stars where the atmosphere makes up a substantial portion of its radius (Heiter and Eriksson 2006). However, since complex interaction of gas particles and the non-local radiation fields leads to deviations from LTE in the atmospheres of FGKM-type stars, some of the softwares have also the option of non-local thermodynamic equilibrium (NLTE). For instance, SME includes NLTE departure coefficients for the MARCS and LL models atmospheres (Piskunov and Valenti 2017), and *Turbospectrum* also have the option of NLTE (Gerber et al. 2023).

Fitting can in several of the softwares be made for one or several parameters at the same time using a  $\chi^2$ -minimization algorithm. However, care must be taken when solving for several parameters simultaneously (Torres et al. 2012) due to degeneracies and difficulties in the modelling. Different initial assumptions of one free parameter at a time can therefore be made in the fitting process to iterate to the final solution, thereby mitigating degeneracies. Also, since the surface gravity is often difficult to constrain it is thus advantageous to have external information about the stellar density that can facilitate modelling.

Spectroscopic modelling can take advantage of the sensitivity of certain spectral lines to specific parameters. For instance, all Balmer lines exhibit pressure (collisionally) broadened line wings which makes their profiles strongly sensitive to temperature (e.g. Fuhrmann et al. 1993, 1994; Barklem et al. 2000, 2002) as shown in Fig. 1. The Balmer line wings are formed in the deepest photospheric layers likely close to the LTE. The metal-line blending increase from  $H\alpha$  at 6562.81 Å to  $H\delta$  at 4101.75 Å which perturb the higher transitions of the Balmer line profiles making  $H\alpha$  the best choice. For late F, G, and early K-stars,  $H\alpha$  is very insensitive to  $\log g_*$  and abundance making its line wings an excellent  $T_{\text{eff}}$  indicator. Two examples of  $H\alpha$  line profiles towards a K5V and a G0V host star are shown in Fig. 1. It is obvious that the line wings have almost completely disappeared in the K5V spectrum, while prominent and very broad towards the G-star. For M-dwarfs where the line wings of  $H\alpha$  are absent, TiO lines can also be used as an  $T_{\text{eff}}$  indicator (Valenti et al. 1998).

For late F- and G-dwarfs there are several pressure-sensitive lines that can be used to constrain  $\log g_*$ : the Mg I triplet at 5167.33 Å, 5172.70 Å and 5183.62 Å (e.g. Fuhrmann et al. 1997; Valenti and Fischer 2005) as shown in Fig. 2, and the Ca I lines at 6122.23 Å and 6162.18 Å (e.g. Gray 2008). For lower gravity or higher temperature, the line wings disappear due to lower photospheric density or ionisa-

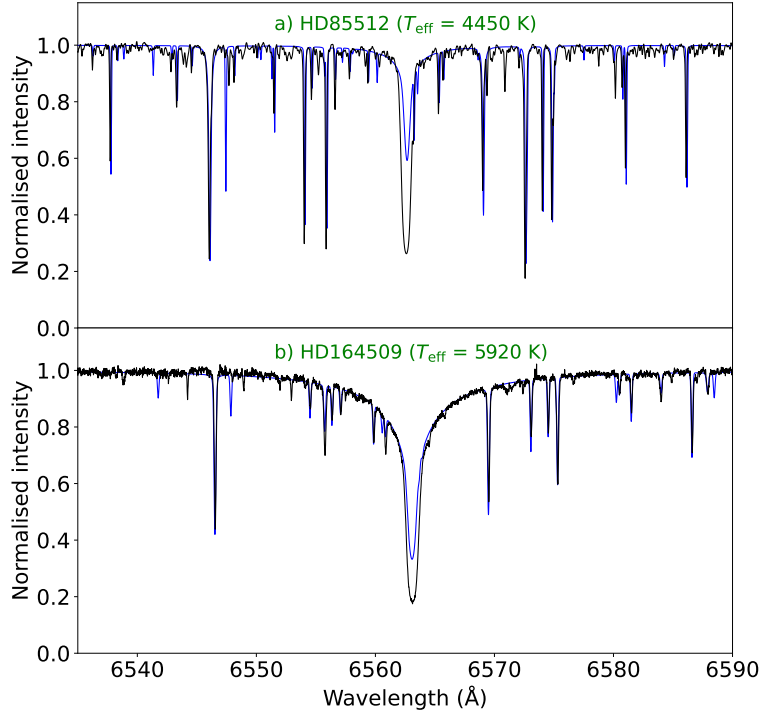


**Fig. 1** Examples of SME modelling of  $H\alpha$  using the MARCS (LTE) stellar atmosphere model towards a K5V (HD85512) and a G0V (HD164509) host star observed with HARPS. The observations are plotted in black and the models in blue. The line *wings* of  $H\alpha$  are very sensitive to the effective temperature. Towards the K5V star they have almost disappeared, while they are very broad towards the G0V star.

tion. The Mg I lines are, however, very wide which makes normalization difficult. Two of the lines lie very close without continuum between them, and there are numerous overlying narrow metal lines in particular for late-type stars. In these cases, only the 5183.62 Å line can be used reliably. Figure 2 shows the Mg I triplet line profiles towards the same host stars as in Fig. 1. As already seen in Fig. 1, the spectral line density is much higher towards the K5V star than the G0V star. However, the effect is even more pronounced at shorter wavelengths. In addition to surface gravity, the Ca and Mg pressure broadened line wings are, however, to some degree also sensitive to temperature and abundance. The procedure is therefore to model the temperature first, e.g. via  $H\alpha$ , and the abundance via narrow, unblended Ca (e.g. 6156.02 Å, 6166.439 Å, 6169.042 Å, 6455.985 Å) and Mg (e.g. 5711.09 Å) lines and iterate to a solution.

The broad line wings of Na I D-lines (5889.97 Å and 5895.94 Å) are sensitive to both  $T_{\text{eff}}$ ,  $\log g_*$  (and the Na abundance). Hence these lines can be used to check the final model for consistency.

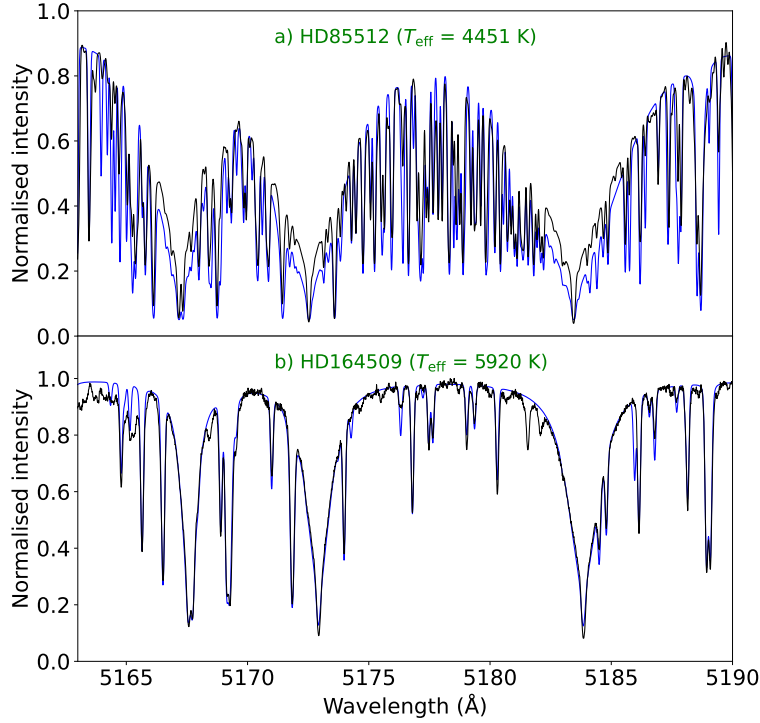


**Fig. 2** Examples of SME modelling of the Mg I triplet (5167.33 Å, 5172.70 Å, and 5183.62 Å) towards the same stars as in Fig. 1. The line *wings* are sensitive to  $\log g_*$ . Note the difference in spectral line density and line blanketing in HD85512 which introduce severe problems in the spectral modelling.

More details and examples of spectral modelling can for instance be found in Valenti and Fischer (2005), Jofré et al. (2014), and Brewer et al. (2016).

### ***Fitting equivalent widths***

In contrast to synthetic spectral synthesis methods, the equivalent width (EW) method begins with the observed spectrum by measuring the strengths of selected absorption lines which are translated into individual line abundances. The method is based on theoretical atmosphere models and excitation and ionisation equilibrium which determines the population in a certain level of an atom or an ion.

The EW of an absorption line is a convenient measurement of its strength. It is defined as the width of a rectangle reaching up to the continuum (with length one) having the same area as the spectral line. Measuring EWs of well-defined weak neutral iron (Fe I) and ionised iron (Fe II) lines is a traditional method to model stellar spectroscopic parameters since there are numerous iron lines in stellar spectra, many

with accurate atomic parameters. Metal lines can be very sensitive to temperature although large variations between lines exist. Depending on spectral type, neutral metals are often used as a temperature indicator in solar-type stars, while ionised metal lines are better tracers in early-type stars.

Assuming LTE, the ratio of population in two levels  $n$  and  $m$  of an atom (or ion) of a species can be computed with the Boltzmann equation (e.g. Gray 2008; Carroll and Ostlie 2017)

$$\frac{N_n}{N_m} = \frac{g_n}{g_m} e^{-(\chi_n - \chi_m)/kT}, \quad (6)$$

where  $g_n$  and  $g_m$  are the statistical weights of the two levels,  $\chi_n$  and  $\chi_m$  are the corresponding excitation potentials,  $k$  is the Boltzmann constant, and  $T$  is the temperature. Different line ratios have different sensitivity to temperature.

As the temperature increases so will ionisation which occurs quite abruptly once the threshold temperature is reached. In a star's photosphere, elements exist mainly in just two ionisation stages which can be computed with the Saha equation (e.g. Gray 2008; Carroll and Ostlie 2017) between ionisation states  $i$  and  $i + 1$  as

$$\frac{N_{i+1}}{N_i} P_e = \frac{(2\pi m_e)^{3/2} (kT)^{5/2}}{h^3} \frac{2u_{i+1}(T)}{u_i(T)} e^{-I/kT}, \quad (7)$$

where the electron pressure is  $P_e = N_e kT$  (indicator of the surface gravity),  $m_e$  is the electron mass,  $h$  is Planck's constant,  $u(T) = \sum g_i e^{-\chi_i/kT}$  is the partition function, and  $I$  is the ionisation energy.

The EW method requires measurements of a large number of equivalent widths either measured by direct integration over the entire line or by fitting a Gaussian profile (or a Lorentzian profile that may fit optically thick lines better). Measuring EWs manually is, however, very time-consuming and therefore several softwares have been developed to automate the measurements for example ARES (Sousa et al. 2007) and DAOSPEC (Stetson and Pancino 2008).

Weak and optically thin iron lines depend mainly on  $T_{\text{eff}}$  and the iron abundance and less on  $\log g_*$  and  $V_{\text{mic}}$ . In order to avoid abundance dependence with the EW method, it is best to choose two lines from the same element. However, since continuum normalisation is often a large source of error it may sometimes be necessary to use pairs of lines at nearby wavelengths. In these cases, pairs of similar elements like Fe, V, and Ti that normally have similar abundances, are often used. Different sets of lines are chosen for different spectral types since they are useful in different temperature ranges.

The effective temperature is constrained in the following modelling by the correlation between the excitation potential and the iron abundance of each individual line, the microturbulence is constrained by the correlation between the abundance of each line and the reduced equivalent width, while the surface gravity is constrained by the ionisation balance. The parameters are adjusted until there are no correlations left and all individual abundances are the same (Sousa 2014).

An example of a widely used open radiative transfer code based on the EW method is MOOG (Sneden 1973). This software uses a grid of the ATLAS9 (Ku-

rucz 1993a) plane-parallel model atmospheres to produce model spectra which is compared to the measured EWs of individual Fe I and Fe II lines. The equilibrium conditions are solved simultaneously to derive  $T_{\text{eff}}$ ,  $\log g_*$ ,  $[\text{Fe}/\text{H}]$ , and  $V_{\text{mic}}$ . A good description of the process is found in Sousa (2014). It has been used by for instance Sousa et al. (2021) together with ARES for a homogeneous spectroscopic characterisation of almost one thousand exoplanet host stars (the SWEET-Cat online catalogue). Another example of a software based on the EW method is ODUSSEAS (Observing Dwarfs Using Stellar Spectroscopic Energy-Absorption Shapes; Antoniadis-Karnavas et al. 2020). This code uses the machine learning Python package scikit-learn to offer a quick and automatic derivation of  $T_{\text{eff}}$  and  $[\text{Fe}/\text{H}]$  for M dwarfs from optical spectroscopy.

When comparing the outcome of the EW and models based on synthetic spectra,  $T_{\text{eff}}$  and  $\log g_*$  normally agree within the uncertainties and also with results from asteroseismology within 100 K and 0.1 dex, respectively. The methods, however, do not perform equally well for all spectral types. Since the EW method is based on differential analysis with respect to the Sun, it can be applied to FGK stars with  $T_{\text{eff}} \approx 4500 - 6400$  K (Sousa et al. 2011). Modelling based on synthetic spectra and the line shapes are also sensitive to spectral type since some of the fundamental traits, e.g. the broad  $\text{H}\alpha$  line wings, can only be made for solar-type stars since the line wings disappear for colder and hotter stars. In these cases it may still, however, be possible to use other spectral lines (e.g. TiO for low-mass stars). Furthermore, the EW method cannot be used on fast-rotator stars because of the severe line blending. For these stars, it may still be possible to use the synthetic method. Another difference is that the EW method is normally much faster than the synthetic method, while synthetic models provide a more complete description of the star.

### ***Empirical methods***

Instead of the above methods, it is also possible to compare an observed high-resolution spectrum to spectra of well-characterised stars and in this way derive stellar parameters. An example of such software is Spechmatch-emp (Yee et al. 2017) that compares an observed optical spectrum with a dense empirical spectral library thereby deriving  $R_*$  (or  $\log g_*$ ),  $T_{\text{eff}}$ , and  $[\text{Fe}/\text{H}]$ . The library contains 404 stars observed with the HIRES instrument with  $R \approx 60000$  at the Keck telescope. The properties of all the library stars have been derived from asteroseismology, interferometry, spectrophotometry and LTE spectral synthesis and represents spectral types from approximately M5 to F1. This method performs very well for the difficult late type stars (K4 stars and later) which are challenging for other methods reaching accuracies of 10 % in stellar radius, 70 K in effective temperature, and 0.09 dex in metallicity ( $[\text{Fe}/\text{H}]$ ). The software and the library are publicly available.

## Stellar radius and mass

Once we have obtained the stellar spectroscopic parameters for our host star we now want to find out the radius and the mass of the star.

### *Radius from spectroscopy and spectral energy distribution*

When spectroscopic parameters and photometric measurements are available it is straightforward to obtain the stellar radius from a fit of the observed magnitudes in different bands to its spectral energy distribution (SED). In addition to magnitudes, the SED also depends on the distance (most accurately computed from the observed parallax), the spectroscopic parameters (derived from spectroscopic modelling), the extinction along the line-of-sight, and the stellar radius which is a free parameter in the fit. Parallax measurements have been performed by the European space missions Hipparchos (van Leeuwen 1997) and Gaia (Gaia Collaboration et al. 2016) launched in 1989 and 2013, respectively. The latter mission have provided the community with astrometric and photometric measurements of almost two billion stars in the Milky Way. Gaia has also delivered excellent measurements of the magnitudes in the Gaia optical band. Observations will end in early 2025. Figure 3 shows an example of a SED fit with the `Phoenix` (Husser et al. 2013) atmospheric model grid. An example of a publicly available software that automatically fits broadband photometry to six different stellar atmosphere models using Nested Sampling algorithms is the `ARIADNE` (Vines and Jenkins 2022) software.

### *Stellar mass*

Unless the star is a binary, the mass cannot usually be determined directly but can be modeled via stellar evolution models. Some of the most popular models are BaSTI (Hidalgo et al. 2018), Padova (Bertelli et al. 2008, 2009), DESP (the Dartmouth Stellar Evolution Database; Dotter et al. 2008), MIST (MESA Isochrones and Stellar Tracks; Choi et al. 2016), PARSEC (the PADova and TRIeste Stellar Evolution Code; Bressan et al. 2012), and  $Y^2$  (Yonsei-Yale; Yi et al. 2003; Demarque et al. 2004). A quick way to obtain a Bayesian estimation of both mass and radius based on PARSEC and MESA (Rodrigues et al. 2017) models are the web interfaces `Param1.3` and `Param1.5` (da Silva et al. 2006). Another publicly available software that provides a simple interface for MCMC fitting of MIST stellar model grids is `isochrones` (Morton 2015).

A complementing method is to use a set of stars with well-known masses and radii, e.g. through interferometry and eclipsing binaries, to derive empirical calibration equations. Such equations can give the mass and radius of a star given a set

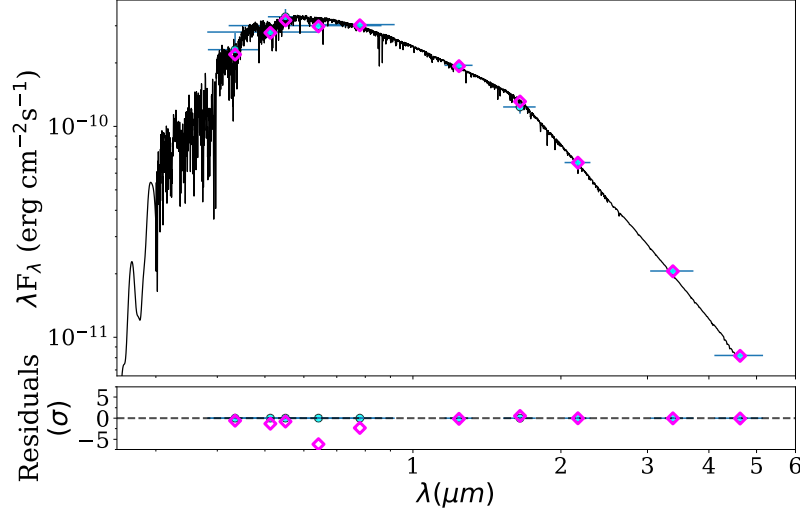


**Fig. 3** Example of a spectral energy distribution (SED) fit of the host star TOI-2196 discovered by the Transiting Exoplanet Survey Satellite (Persson et al. 2022). The observed photometric measurements are plotted with blue circles and the effective width of the passband are represented with horizontal bars. The *Phoenix* (Husser et al. 2013) atmosphere model is outlined in black and the magenta diamond symbols are the corresponding model fluxes.

of stellar atmosphere values (e.g. Torres et al. 2010; Enoch et al. 2010; Southworth 2011).

### Final checks

If a planet is transiting a final important check can be made. The stellar density obtained from the above radius and mass can be checked against the density obtained from transit photometry and Kepler’s third law. Assuming a circular orbit we have (Seager and Mallén-Ornelas 2003)

$$\rho_{\star} = \frac{3\pi}{GP_{\text{rot}}^2} \left( \frac{a}{R_{\star}} \right)^3, \quad (8)$$

where  $G$  is the gravitational constant,  $P_{\text{rot}}$  is the orbital period,  $a$  is the semi-major axis, and  $R_{\star}$  is the stellar radius. If this density does not agree with the above derived value, you need to check your modelling again. Equation 8 can be modified to include the eccentricity if known (e.g. Tingley et al. 2011).

Another checkpoint is to compare the stellar mass computed from the spectroscopic  $\log g_{\star}$  combined with  $R_{\star}$  which should be consistent with the final mass from other methods.

A final remark: if possible, it is best to use several methods to make sure that the derived stellar parameters are robust and consistent.

## References

- Acuña L, Deleuil M Mousis O (2023) Interior-atmosphere modelling to assess the observability of rocky planets with JWST. *A&A*677:A14
- Ahumada R, Allende Prieto C, Almeida A et al. (2020) The 16th Data Release of the Sloan Digital Sky Surveys: First Release from the APOGEE-2 Southern Survey and Full Release of eBOSS Spectra. *ApJS*249(1):3
- Ahumada R, Allende Prieto C, Almeida A et al (2022) VizieR Online Data Catalog: Sloan Digital Sky Surveys (SDSS), Release 16 (DR16) (Ahumada+, 2020). VizieR On-line Data Catalog: V/154. Originally published in: 2020ApJS..249....3A
- Alonso A, Arribas S Martinez-Roger C (1996) The empirical scale of temperatures of the low main sequence (F0V-K5V). *A&A*313:873–890
- Andersen J (1991) Accurate masses and radii of normal stars. *A&A* Rev3(2):91–126
- Antoniadis-Karnavas A, Sousa SG, Delgado-Mena E et al. (2020) ODUSSEAS: a machine learning tool to derive effective temperature and metallicity for M dwarf stars. *A&A*636:A9
- Asplund M, Grevesse N, Sauval AJ Scott P (2009) The Chemical Composition of the Sun. *ARA&A*47(1):481–522
- Barklem PS, Piskunov N O’Mara BJ (2000) Self-broadening in Balmer line wing formation in stellar atmospheres. *A&A*363:1091–1105
- Barklem PS, Stempels HC, Allende Prieto C et al. (2002) Detailed analysis of Balmer lines in cool dwarf stars. *A&A*385:951–967
- Bell RA Gustafsson B (1989) The effective temperatures and colours of G and K stars. *MNRAS*236:653–708
- Bertelli G, Girardi L, Marigo P Nasi E (2008) Scaled solar tracks and isochrones in a large region of the Z-Y plane. I. From the ZAMS to the TP-AGB end for 0.15-2.5  $\{M\}_{\odot}$  stars. *A&A*484(3):815–830
- Bertelli G, Nasi E, Girardi L Marigo P (2009) Scaled solar tracks and isochrones in a large region of the Z-Y plane. II. From 2.5 to 20  $M_{\odot}$  stars. *A&A*508(1):355–369
- Blackwell DE Shallis MJ (1977) Stellar angular diameters from infrared photometry. Application to Arcturus and other stars; with effective temperatures. *MNRAS*180:177–191
- Blackwell DE, Petford AD Shallis MJ (1980) Use of the infra-red flux method for determining stellar effective temperatures and angular diameters; the stellar temperature scale. *A&A*82:249–252
- Blackwell DE, Petford AD, Arribas S, Haddock DJ Selby MJ (1990) Determination of temperatures and angular diameters of 114 F-M stars using the infrared flux method (IRFM). *A&A*232:396
- Blanco-Cuaresma S (2019) Modern stellar spectroscopy caveats. *MNRAS*486(2):2075–2101
- Blanco-Cuaresma S, Soubiran C, Heiter U Jofré P (2014) Determining stellar atmospheric parameters and chemical abundances of FGK stars with iSpec. *A&A*569:A111
- Bressan A, Marigo P, Girardi L et al. (2012) PARSEC: stellar tracks and isochrones with the Padova and TRIESTE Stellar Evolution Code. *MNRAS*427:127–145
- Brewer JM, Fischer DA, Valenti JA Piskunov N (2016) Spectral Properties of Cool Stars: Extended Abundance Analysis of 1,617 Planet-search Stars. *ApJS*225:32
- Bruntt H, Bedding TR, Quirion PO et al. (2010) Accurate fundamental parameters for 23 bright solar-type stars. *MNRAS*405:1907–1923
- Carroll BW Ostlie DA (2017) An introduction to modern astrophysics, Second Edition
- Casagrande L, Portinari L Flynn C (2006) Accurate fundamental parameters for lower main-sequence stars. *MNRAS*373(1):13–44



- Casagrande L, Ramírez I, Meléndez J, Bessell M Asplund M (2010) An absolutely calibrated  $T_{\text{eff}}$  scale from the infrared flux method. Dwarfs and subgiants. *A&A*512:A54
- Choi J, Dotter A, Conroy C et al. (2016) Mesa Isochrones and Stellar Tracks (MIST). I. Solar-scaled Models. *ApJ*823(2):102
- Christlieb N, Gustafsson B, Korn AJ et al. (2004) HE 0107-5240, a Chemically Ancient Star. I. A Detailed Abundance Analysis. *ApJ*603(2):708–728
- Cosentino R, Lovis C, Pepe F et al. (2012) Harps-N: the new planet hunter at TNG. In: Ground-based and Airborne Instrumentation for Astronomy IV, Proc SPIE, vol 8446, p 84461V, DOI 10.1117/12.925738
- da Silva L, Girardi L, Pasquini L et al. (2006) Basic physical parameters of a selected sample of evolved stars. *A&A*458:609–623
- de Laverny P, Recio-Blanco A, Worley CC Plez B (2012) The AMBRE project: A new synthetic grid of high-resolution FGKM stellar spectra. *A&A*544:A126
- Demarque P, Woo JH, Kim YC Yi SK (2004)  $Y^2$  Isochrones with an Improved Core Overshoot Treatment. *ApJS*155(2):667–674
- Dorn C, Khan A, Heng K et al. (2015) Can we constrain the interior structure of rocky exoplanets from mass and radius measurements? *A&A*577:A83
- Dotter A (2016) MESA Isochrones and Stellar Tracks (MIST) 0: Methods for the Construction of Stellar Isochrones. *ApJS*222(1):8
- Dotter A, Chaboyer B, Jevremović D et al. (2008) The Dartmouth Stellar Evolution Database. *ApJS*178:89–101
- Doyle AP, Davies GR, Smalley B, Chaplin WJ Elsworth Y (2014) Determining stellar macroturbulence using asteroseismic rotational velocities from Kepler. *MNRAS*444:3592–3602
- Eisenhauer F, Monnier JD Pfuhl O (2023) Advances in Optical/Infrared Interferometry. *ARA&A*61:237–285
- Enoch B, Collier Cameron A, Parley NR Hebb L (2010) An improved method for estimating the masses of stars with transiting planets. *A&A*516:A33
- Fuhrmann K, Axer M Gehren T (1993) Balmer lines in cool dwarf stars. I. Basic influence of atmospheric models. *A&A*271:451
- Fuhrmann K, Axer M Gehren T (1994) Balmer lines in cool dwarf stars II. Effective temperatures and calibration of colour indices. *A&A*285:585–594
- Fuhrmann K, Pfeiffer M, Frank C, Reetz J Gehren T (1997) The surface gravities of cool dwarf stars revisited. *A&A*323:909–922
- Gaia Collaboration, Prusti T, de Bruijne JHJ et al. (2016) The Gaia mission. *A&A*595:A1
- Gerber JM, Magg E, Plez B et al. (2023) Non-LTE radiative transfer with Turbospectrum. *A&A*669:A43
- Gray DF (2008) The Observation and Analysis of Stellar Photospheres. Cambridge University Press
- Gray RO Corbally CJ (1994) The Calibration of MK Spectral Classes Using Spectral Synthesis. I. The Effective Temperature Calibration of Dwarf Stars. *AJ*107:742
- Grevesse N, Asplund M Sauval AJ (2007) The Solar Chemical Composition. *Space Sci Rev*130(1–4):105–114
- Gustafsson B, Edvardsson B, Eriksson K et al. (2008) A grid of MARCS model atmospheres for late-type stars. I. Methods and general properties. *A&A*486:951–970
- Heiter U Eriksson K (2006) Geometry of giant star model atmospheres: a consistency test. *A&A*452(3):1039–1048
- Heiter U, Kupka F, van't Veer-Menneret C et al. (2002) New grids of ATLAS9 atmospheres I: Influence of convection treatments on model structure and on observable quantities. *A&A*392:619–636
- Hidalgo SL, Pietrinferni A, Cassisi S et al. (2018) The Updated BaSTI Stellar Evolution Models and Isochrones. I. Solar-scaled Calculations. *ApJ*856(2):125
- Husser TO, Wende-von Berg S, Dreizler S et al. (2013) A new extensive library of PHOENIX stellar atmospheres and synthetic spectra. *A&A*553:A6
- Jofré P, Heiter U, Soubiran C et al. (2014) Gaia FGK benchmark stars: Metallicity. *A&A*564:A133

- Kurucz R (1993a) ATLAS9 Stellar Atmosphere Programs and 2 km/s grid. ATLAS9 Stellar Atmosphere Programs and 2 km/s grid Kurucz CD-ROM No 13 Cambridge, Mass: Smithsonian Astrophysical Observatory, 1993 13
- Kurucz R (1993b) SYNTHE Spectrum Synthesis Programs and Line Data. SYNTHE Spectrum Synthesis Programs and Line Data Kurucz CD-ROM No 18 Cambridge, Mass: Smithsonian Astrophysical Observatory, 1993 18
- Kurucz RL (2013) ATLAS12: Opacity sampling model atmosphere program. Astrophysics Source Code Library
- Li H, Aoki W, Matsuno T et al. (2022) Four-hundred Very Metal-poor Stars Studied with LAMOST and Subaru. II. Elemental Abundances. *ApJ*931(2):147
- Lodders K (2003) Solar System Abundances and Condensation Temperatures of the Elements. *ApJ*591(2):1220–1247
- Mayor M Queloz D (1995) A Jupiter-mass companion to a solar-type star. *Nature*378:355–359
- Mayor M, Pepe F, Queloz D et al. (2003) Setting New Standards with HARPS. *The Messenger* 114:20–24
- Mignon L, Meunier N, Delfosse X et al. (2023) Characterisation of stellar activity of M dwarfs. I. Long-timescale variability in a large sample and detection of new cycles. *A&A*675:A168
- Mihalas D (1978) Stellar atmospheres
- Morton TD (2015) isochrones: Stellar model grid package
- Nepal S, Chiappini C, Guiglion G et al. (2024) Insights from super-metal-rich stars: Is the Milky Way bar young? *A&A*681:L8
- Nordström B, Mayor M, Andersen J et al. (2004) The Geneva-Copenhagen survey of the Solar neighbourhood. Ages, metallicities, and kinematic properties of  $\sim 14\,000$  F and G dwarfs. *A&A*418:989–1019
- Pepe F, Cristiani S, Rebolo R et al. (2021) ESPRESSO at VLT. On-sky performance and first results. *A&A*645:A96
- Persson CM, Georgieva IY, Gandolfi D et al. (2022) TOI-2196 b: Rare planet in the hot Neptune desert transiting a G-type star. *A&A*666:A184
- Piskunov N Valenti JA (2017) Spectroscopy Made Easy: Evolution. *A&A*597:A16
- Piskunov NE, Kupka F, Ryabchikova TA, Weiss WW Jeffery CS (1995) VALD: The Vienna Atomic Line Data Base. *A&AS*112:525
- Plez B (2012) Turbospectrum: Code for spectral synthesis. Astrophysics Source Code Library, record ascl:1205.004
- Quirrenbach A (2001) Optical Interferometry. *ARA&A*39:353–401
- Rodrigues TS, Bossini D, Miglio A et al. (2017) Determining stellar parameters of asteroseismic targets: going beyond the use of scaling relations. *MNRAS*467(2):1433–1448
- Ryabchikova T, Piskunov N, Kurucz RL et al. (2015) A major upgrade of the VALD database. *Phys Scr*90(5):054005
- Seager S Mallén-Ornelas G (2003) A Unique Solution of Planet and Star Parameters from an Extrasolar Planet Transit Light Curve. *ApJ*585:1038–1055
- Serenelli A, Weiss A, Aerts C et al. (2021) Weighing stars from birth to death: mass determination methods across the HRD. *A&A Rev*29(1):4
- Shulyak D, Tsymbal V, Ryabchikova T, Stütz C Weiss WW (2004) Line-by-line opacity stellar model atmospheres. *A&A*428:993–1000
- Snedden CA (1973) Carbon and Nitrogen Abundances in Metal-Poor Stars. PhD thesis, University of Texas, Austin
- Sousa SG (2014) ARES + MOOG: A Practical Overview of an Equivalent Width (EW) Method to Derive Stellar Parameters. In: Determination of Atmospheric Parameters of B, pp 297–310, DOI 10.1007/978-3-319-06956-2\_26
- Sousa SG, Santos NC, Israelian G, Mayor M Monteiro MJPG (2007) A new code for automatic determination of equivalent widths: Automatic Routine for line Equivalent widths in stellar Spectra (ARES). *A&A*469:783–791

- Sousa SG, Santos NC, Israelian G, Mayor M, Udry S (2011) Spectroscopic stellar parameters for 582 FGK stars in the HARPS volume-limited sample. Revising the metallicity-planet correlation. *A&A*533:A141
- Sousa SG, Adibekyan V, Delgado-Mena E et al. (2021) SWEET-Cat 2.0: The Cat just got SWEETer. Higher quality spectra and precise parallaxes from Gaia eDR3. *A&A*656:A53
- Southworth J (2011) Homogeneous studies of transiting extrasolar planets - IV. Thirty systems with space-based light curves. *MNRAS*417:2166–2196
- Stetson PB, Pancino E (2008) DAOSPEC: An Automatic Code for Measuring Equivalent Widths in High-Resolution Stellar Spectra. *PASP*120(874):1332
- Teltel JH, Avila G, Buchhave L et al. (2014) FIES: The high-resolution Fiber-fed Echelle Spectrograph at the Nordic Optical Telescope. *Astronomische Nachrichten* 335:41
- Tingley B, Bonomo AS, Deeg HJ (2011) Using Stellar Densities to Evaluate Transiting Exoplanetary Candidates. *ApJ*726(2):112
- Tokovinin A, Fischer DA, Bonati M et al. (2013) CHIRON—A Fiber Fed Spectrometer for Precise Radial Velocities. *PASP*125(933):1336
- Torres G, Andersen J, Giménez A (2010) Accurate masses and radii of normal stars: modern results and applications. *A&A Rev*18(1-2):67–126
- Torres G, Fischer DA, Sozzetti A et al. (2012) Improved Spectroscopic Parameters for Transiting Planet Hosts. *ApJ*757(2):161
- Tull RG, MacQueen PJ, Sneden C, Lambert DL (1995) The high-resolution cross-dispersed echelle white-pupil spectrometer of the McDonald Observatory 2.7-m telescope. *PASP*107:251–264
- Valenti JA, Fischer DA (2005) Spectroscopic Properties of Cool Stars (SPOCS). I. 1040 F, G, and K Dwarfs from Keck, Lick, and AAT Planet Search Programs. *ApJS*159:141–166
- Valenti JA, Piskunov N (1996) Spectroscopy made easy: A new tool for fitting observations with synthetic spectra. *A&AS*118:595–603
- Valenti JA, Piskunov N, Johns-Krull CM (1998) Spectral Synthesis of TiO Lines. *ApJ*498(2):851–862
- van Leeuwen F (1997) The HIPPARCOS Mission. *Space Sci Rev*81:201–409
- Vines JI, Jenkins JS (2022) ARIADNE: measuring accurate and precise stellar parameters through SED fitting. *MNRAS*513(2):2719–2731
- Vogt SS, Allen SL, Bigelow BC et al. (1994) HIRES: the high-resolution echelle spectrometer on the Keck 10-m Telescope. In: Crawford DL, Craine ER (eds) *Instrumentation in Astronomy VIII*, Society of Photo-Optical Instrumentation Engineers (SPIE) Conference Series, vol 2198, p 362, DOI 10.1117/12.176725
- Wehrhahn A, Piskunov N, Ryabchikova T (2023) PySME. Spectroscopy Made Easier. *A&A*671:A171
- Yee SW, Petigura EA, von Braun K (2017) Precision Stellar Characterization of FGKM Stars using an Empirical Spectral Library. *ApJ*836:77
- Yi SK, Kim YC, Demarque P (2003) The  $Y^2$  Stellar Evolutionary Tracks. *ApJS*144(2):259–261